Korean J. of Chem. Eng., **10**(3), 182-187 (1993)

A COMPUTER MODELLING OF FLOWFIELD AND SOLIDIFICATION IN ROTATING BANK OF TWIN-ROLL STRIP CASTING

Sung-Woo Lee

Research Institute of Machinery & Electronics, Samsung Heavy Industries,
69 Sinchon-Dong, Changwon 641-790, Korea
(Received 10 May 1993 • accepted 22 July 1993)

Abstract—A computer model has been developed for describing the flowfields of molten steel (SUS 304) in the twin-roll strip casting process with solidification pattern. The governing equations were transformed to a curvilinear coordinate system and an outline of the computational approach was also given. It was found that the flowfields with recirculating flow are located in the vicinity of the middle of the rotating bank of molten steel. The small cavity zone with fixed operation parameters appears with the nozzle depth increased.

INTRODUCTION

If sheet or strip can be produced directly from the molten metal by combining the casting and hot rolling into a single casting process just as a replacement for conventional continuous casting machines, the costly intermediate stages of ingot casting, primary rolling, reheating and some secondary rolling will be eliminated, and there can be substantial savings of capital, energy, operations and labour [1-5]. Continuous casting of aluminum and copper strip is being done commercially production. However, continuous casting of steel strip poses problems of higher temperature, more reactive melts and mechanically tougher solidified material. Figure 1 shows a schematic diagram of typical twin-roll strip casting process. The casting procedure for steel strips has been solidified using the twin-roll (which are water cooled), and the rapidly solidified strips pass out the nip of roller.

Understanding of the fundamental phenomena of the mechanisms responsible for the behaviour of rotating bank in this process is limited, but such knowledge is extensively exploited to enhance the optimal operating condition and process development [6-10]. Direct measurements of the flowfields are very difficult because the flowfield of steel is opaque and high temperature. Another problem in using these cooling twin-roll devices for molten steel is the difficulty of analysis of solidification phenomena in the rotating bank necessary to predict the life of twin-roller components. Also, since hot rolling is performed on the steel strip, large stresses are put on the rolls. The rolls must be able to withstand both the thermal cycling and the mechanical stresses involved.

This paper presents the mathematical modelling of twin-roll process, and then the model which is simulated in practical geometry. This model treats the molten metal flowfields as non-isothermal and analyses the solidification phenomena in the region of rotating bank. Then it discusses the computed results. The

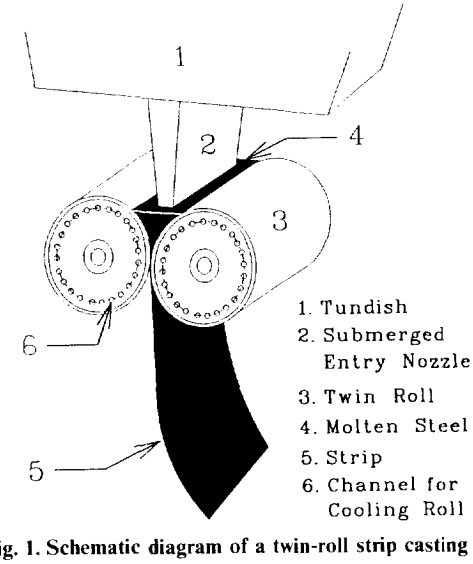

Fig. 1. Schematic diagram of a twin-roll strip casting process.

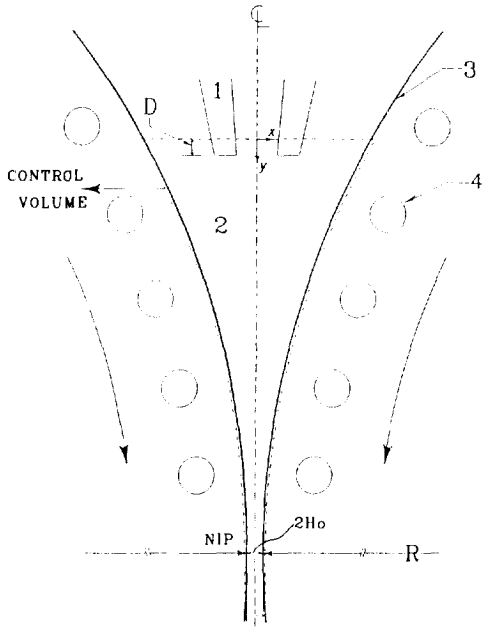

Fig. 2. Schematic representation of twin-roll strip casting process for a mathematical modelling.

predicted results provide a quantitative relationship between the principal operation parameter, such as depth of the submerged entry nozzle, with special attention to the starting point of strip production.

MATHEMATICAL FORMULATION

1. Problem description and governing equations

An idealised model geometry with the coordinate system is schematically shown in Figure 2 with the control volume indicated by the dotted line. The molten steel stream of 2W is fed from upstream into the gap of the twin counter rotating rollers with cooling channels, each having a roll speed ω. Major assumptions employed in the mathematical model are:

(1) the flowfield can be taken to be two dimensional axi-symmetric and incompressible.

(2) the rollers are not deformable and are both rotating at the same speed.

(3) there is no slip between the molten steel and the rotating rollers.

The governing equations to describe the rotating bank of molten steel in the system can be expressed in a Cartesian system:

mass conservation

$$\frac{\partial U}{\partial x}+\frac{\partial V}{\partial y}=0 \tag{1}$$

where U and V are the velocities in the x and y directions, respectively.

momentum conservation

$$\frac{\partial}{\partial t}(\rho U)+\mathrm{div}(\rho UU)=\mathrm{div}(\mu\ \mathrm{grad}\ U)-\frac{\partial P}{\partial x}+S_x \tag{2}$$

$$\frac{\partial}{\partial t}(\rho V)+\mathrm{div}(\rho UV)=\mathrm{div}(\mu\ \mathrm{grad}\ V)-\frac{\partial P}{\partial y}+S_y \tag{3}$$

where P is pressure, ρ density, μ viscosity and S_x and S_y are source terms which need to be defined. If μ is made a function of the representative latent heat, mushy region can be treated with variable viscosity [12]. In this model, however, μ is considered with constant.

heat conservation

$$\frac{\partial}{\partial t}(\rho h)+\mathrm{div}(\rho Uh)=\mathrm{div}(\alpha\ \mathrm{grad}\ h)+S_h \tag{4}$$

where α is the thermal diffusivity and S_h is a source term. In solidification problem the source term S_h depend on the nature of the latent heat evolution and require definition. In the solidification of alloys one may define the mushy zone, the two-phase region between the liquidus and the solidus temperatures. Therefore, the total heat contribution, H, is expressed as

$$H=h+\Delta H \tag{5}$$

where h is sensible heat and ΔH is latent heat. The ΔH will some function of temperature [11, 12].

$$H=\begin{cases}\Delta H+C_p(T-T_l), & T>T_l\\ \Delta H(1-f_s), & T_s<T<T_l\\ C_p(T-T_s), & T<T_s\end{cases} \tag{6}$$

where f_s is the solid fraction, which may be a non-linear of temperature as defined by the phase diagram of the system.

Therefore, the form of the enthalpy source term S_h is derived from the enthalpy formulation of convection/diffusion phase change.

$$\rho\frac{\partial H}{\partial t}+\mathrm{div}(\rho UH)=\mathrm{div}(k\ \mathrm{grad}\ T) \tag{7}$$

Then on comparison with Eq. (4) and Eq. (7), S_h is as following:

Table 1. Numerical values of parameters used in this computation

C_p	heat capacity, J/kg K	681.45
ΔH	latent heat, J/kg	2.6×10^5
k	thermal conductivity, W/m K	29.9
R	radius of rotating roll, m	0.75
H_0	roll spacing, m	1.6×10^{-3}
W	half of meniscus, m	0.7
ρ	density of molten steel, kg/m^3	7200
μ	molecular viscosity of molten steel, kg/ms	6.4×10^{-3}
T_{in}	inlet temperature from nozzle, C	1600
T_l	liquidus temperature, C	1531
T_s	solidus temperature, C	1525
T_r	temperature of cooling water in channel, C	25
ω	speed of rotating roll, rpm	18
h_r	heat transfer coefficient, W/m^2 K	10^4

$$-S_n=\rho\frac{\partial\Delta H}{\partial t}+\mathrm{div}(\rho U\Delta H) \tag{8}$$

2. Boundary conditions

The following boundary conditions were used for the numerical computation of this system:

(1) near the inlet from the nozzle,

$$U=V=0,\ T=T_{in}$$

(2) at the outlet from the nip point,

$$U=0,\ V=V_{out},\ \frac{\partial T}{\partial x}=0$$

(3) at the axis,

$$\frac{\partial U}{\partial x}=\frac{\partial V}{\partial x}=\frac{\partial T}{\partial x}=0$$

(4) at the meniscus,

$$\frac{\partial U}{\partial y}=0,\ V=0,\ T=T_{in}$$

(5) at the roll surface,

$$U=(y-y_n)\omega,\ V=-(x-x_n)\omega\quad k\ \mathrm{grad}\ T=h_r(T-T_r)$$

In this system, in order to get a flowfield and solidification phenomena near rollers, where steep cross flow gradients exit, a fine grid is used. The V-component of velocity is then readjusted slightly at each iteration so as to ensure overall mass conservation as compared with inlet flow. A detailed description of particular thermal data employed here is presented in reference [4]. The system parameters and material properties used in the calculation are given in Table 1.

NUMERICAL SOLUTION PROCEDURE

For a variable Φ, where Φ may be unit (mass conservation), u and v (momentum conservation), T (energy conservation), etc., the governing equations are transformed to a casted general curvilinear coordinate system (ξ, η) as following equation:

$$\frac{\partial}{\partial t}\left(\frac{\rho}{J}\Phi\right)+\frac{\partial}{\partial\xi}\left[\frac{1}{J}\left(\rho G_\eta\Phi-\Gamma_\Phi g_{11}\frac{\partial\Phi}{\partial\xi}\right)\right]+\frac{\partial}{\partial\eta}\left[\frac{1}{J}\left(\rho G_\xi\Phi-\Gamma_\Phi g_{22}\frac{\partial\Phi}{\partial\eta}\right)\right]=-\frac{\partial}{\partial\xi}\left(\frac{\Gamma_\Phi}{J}g_{12}\frac{\partial\Phi}{\partial\eta}\right)+\frac{\partial}{\partial\eta}\left(\frac{\Gamma_\Phi}{J}g_{12}\frac{\partial\Phi}{\partial\xi}\right)+\frac{S_\Phi}{J}$$

where Γ_Φ and S_Φ denote the local exchange coefficient of variable Φ, and the terms that are not included in convection and diffusion terms. For different variables, Γ_Φ and S_Φ have different contents [13, 14, 17]. Also,

$$g_{11}=\left(\frac{\partial x}{\partial\eta}\right)^2+\left(\frac{\partial y}{\partial\eta}\right)^2,\ g_{22}=\left(\frac{\partial x}{\partial\xi}\right)^2+\left(\frac{\partial y}{\partial\xi}\right)^2,$$

$$g_{12}=\left(\frac{\partial x}{\partial\xi}\frac{\partial x}{\partial\eta}+\frac{\partial y}{\partial\xi}\frac{\partial y}{\partial\eta}\right),\ J^{-1}=\left(\frac{\partial x}{\partial\xi}\frac{\partial y}{\partial\eta}-\frac{\partial x}{\partial\eta}\frac{\partial y}{\partial\xi}\right)$$

$$G_\eta=U\frac{\partial y}{\partial\eta}+V\frac{\partial x}{\partial\eta}\quad\text{and}\quad G_\xi=V\frac{\partial x}{\partial\xi}+U\frac{\partial y}{\partial\xi},$$

where J is the Jacobian of the transformation between a given physical domain and corresponding transformed domain.

Two main features of the solution method used here are employment of the finite volume formulation and the algorithm SIMPLE-C [15-17].

The representation of equation for $\Phi=U$, V, P and T is then solved by the algorithm SIMPLE-C. The iterative method of solution employed is a double sweep of TDMA (Tri-Diagonal Matrix Algorithm) [18].

In grid generation forty grid lines were used in the axial direction while ninety-one grid lines were employed in the width direction after some grid dependence tests undertaken with various mesh system was studied. The computations were carried out using a CRAY Y-MP4E/464 Supercomputer; the CPU time involved in the caculation was in the range of 9 to 10 hours per case for 10 revolutions of rotating roll.

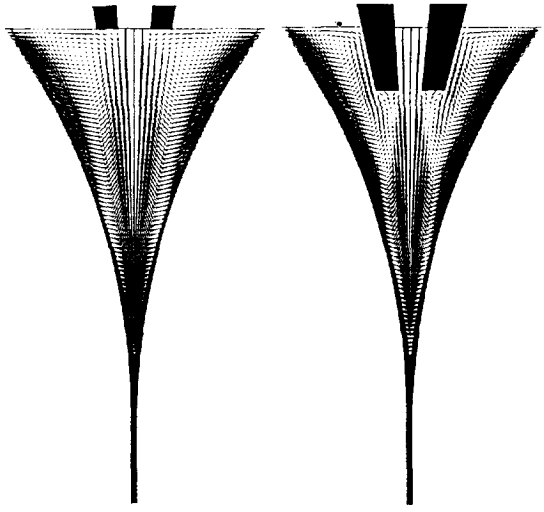

(a) (b)

Fig. 3(a). Velocity vectors in rotating bank for D=0(m).
Fig. 3(b). Velocity vectors in rotating bank for D=3.4×10^{-2}(m).

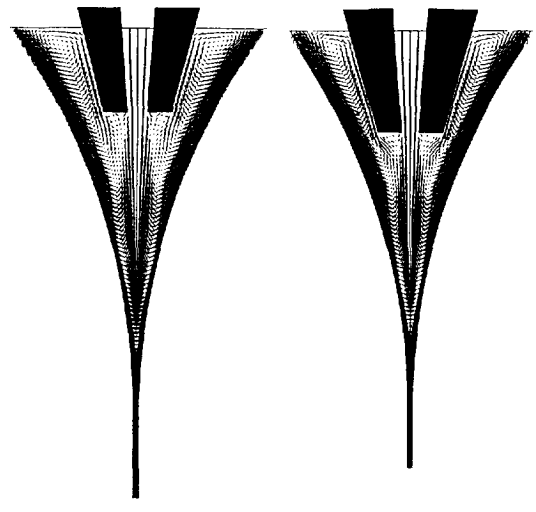

(c) (d)

Fig. 3(c). Velocity vectors in rotating bank for D=4.6×10^{-2}(m).
Fig. 3(d). Velocity vectors in rotating bank for D=5.8×10^{-2}(m).

COMPUTED RESULTS AND DISCUSSION

The primary purpose of the computation was to predict the velocity fields and the solidification phenomena in the rotating bank. It is of interest to compare how the physical depth of the submerged entry nozzle would affect these considerations. The intention here is to illustrate the sensitivity of the system to the values of various submerging depths.

The computed velocity vector for $H_n=1.6\times10^{-3}$ m is shown as a function of the depth of nozzle, D, in Figure 3, respectively. The flow patterns in the molten steel pool show that there is a large region of recirculating flow centred in the middle of the rotating bank of the molten steel pool as shown in Figure 3(a). Figure 3(b), 3(c) and 3(d) show the predicted velocity vector for $D=3.4\times10^{-2}$ m, 4.6×10^{-2} m and 5.8×10^{-2} m as an operating parameter. Near the mid-plane fluid moves away from the nip of the rollers because the volocity components are negative but near the roll. The surface velocity components are positive and the fluid moves toward the nip. Also, it can be seen that the molten steel stream exhibits a dragging character in the vicinity of the roll surface with the axial velocity component having a parabolic profile. As seen in Figure 3(b) and 3(c), the small recirculating zone appears from the rotating bank when a submerged depth is operated, which generates near the outlet position of submerged entry nozzle. The region causes the formation of a dead cavity of molten steel in the rotating bank. Within the foaming cavity, the deposition and the accompanying generation of non-metallic inclusions can be expected.

Figure 4 shows the contours of streamlines for Figure 3. With this computed results, in addition, the entire volume of rotating bank is not effectively utilised (as indicated by the stagnant regions). With this computed results, the characteristics of flowfields within the rotating bank with the submerged nozzle on functioning depth of the nozzle is shown as the result of the presence of recirculating flows and a stagnant region at the tip of submerged entry nozzle.

Figure 5 shows the isolines of solidus and liquidus for Figure 4(b), typically: the mushy region between liquidus (=1531℃) and solidus (=1525℃) is predicted. It is shown from this figure that the thickness of solidified shell to the molten steel is negligibly small under the present casting condition. The isothermal lines are closely concentrated only in the vicinity of the rotating rollers.

Figure 6 shows a relationship between submerged nozzle depth and height from the nip point. As shown in figure, the height from nip point increases linearly with the submerged nozzle depth. The gradient becomes larger with a solidus point. That is, the control of the submerged nozzle depth is an important parameter, particularly when the stable operation with a fi-

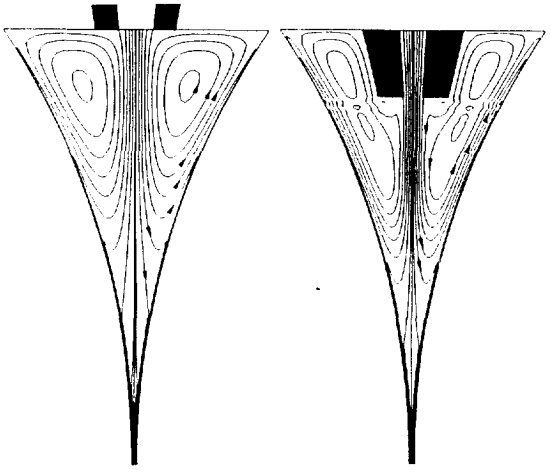

(a) (b)

Fig. 4(a). Streamlines in rotating bank for Figure 3(a).
Fig. 4(b). Streamlines in rotating bank for Figure 3(b).

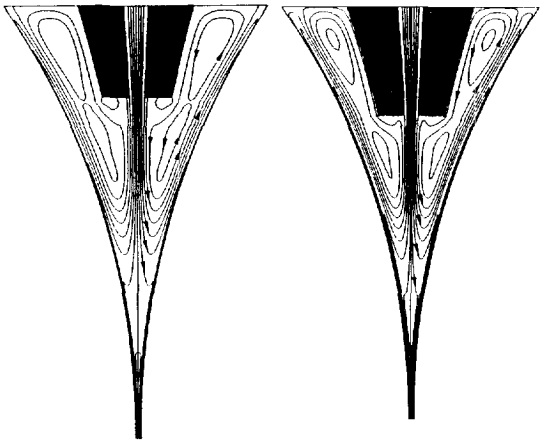

(c) (d)

Fig. 4(c). Streamlines in rotating bank for Figure 3(c).
Fig. 4(d). Streamlines in rotating bank for Figure 3(d).

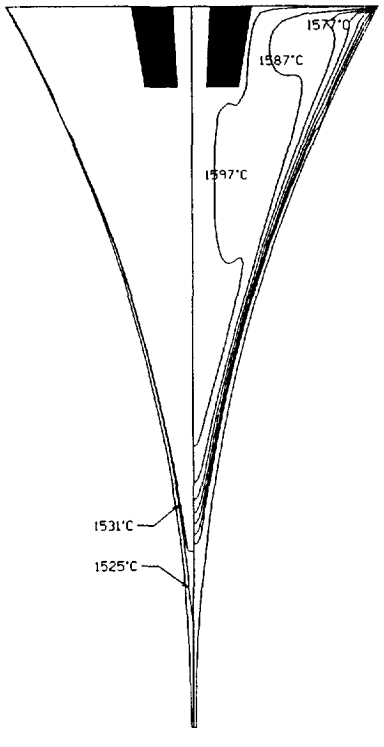

Fig. 5. Mushy region and iso-thermal lines in rotating bank for Figure 4(b), typically.

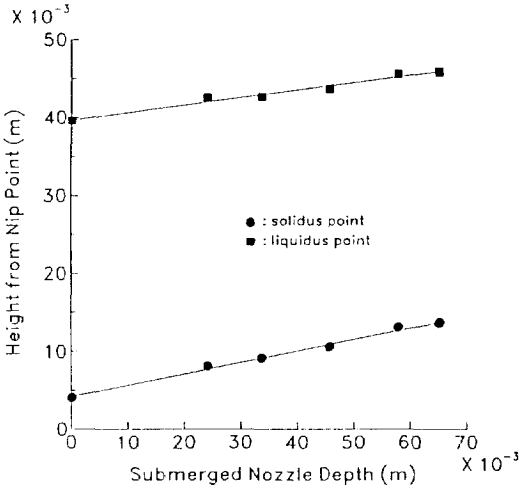

Fig. 6. Relationship between submerged nozzle depth and height from nip point for liquidus and solidus.

xed speed of roll is needed.

CONCLUSIONS

A computer model has been developed to predict the flowfield and solidification phenomena of a molten steel (SUS 304) in a twin-roll strip casting process. The computation using the incompressible Navier-Stokes equation and the energy conservation equation has been applied, and predicted results are presented, describing the evolution of the velocity fields and solidification pattern.

(1) The flowfield of the rotating bank between the twin-rollers was successfully simulated by using a transformed curvilinear coordinate system.

(2) In the flowfield a recirculating region is located in the vicinity of the middle of the rotating bank of

molten steel. A small cavity zone appears at a tip of the nozzle when a submerged nozzle is used.

(3) In addition, this mathematical model including the solidification phenomena of the cast strip for the prediction of the end point of solidification made a valuable contribution to more exact computer modelling work, and the thermal fields computed will provide to predict the thermal stress of cooling rolls and the roll separating force.

ACKNOWLEDGEMENTS

The author from the Samsung Heavy Industries (Korea) thank Supercomputer Centre for provision of Cray Y-MP4E/464 supercomputer time in this research.

NOMENCLATURE

C_p : heat capacity [J/kg K]
D : depth of submerged entry nozzle [m]
f_s : solid fraction
g : gravitational acceleration [m^3/s]
g_{11}, g_{22}, g_{12} : geometric relations between coordinate [m]
G_ξ, G_η: velocity component along ξ and η axes [m/s]
h : sensible enthalpy [J/kg]
ΔH : latent heat [J/kg]
H : total enthalpy [J/kg]
H_n : roll spacing coordinate [m]
J : Jacobian of inverse coordinate transformation
k : thermal conductivity [W/m K]
p : pressure [kg/ms^2]
R : radius of roll [m]
S : source term in governing equations on transformed plane
T : temperature [K]
U, V : velocity component along x and y axes [m/s]
W : half width of meniscus [m]
ξ, η : axes of curvilinear coordinates system [m]
Φ : dependent variable
ρ : density [kg/m^3]
Γ : effective diffusion coefficient
ω : rotating speed of roll [rpm]

Subscript

l, s : for liquidus and solidus

REFERENCES

1. Flinn, J. E.: "Rapid Solidification Technology for Reduced Consumption of Strategic Materials", Noyes Publications Park Ridge, New Jersey, 1985.
2. Jones, H.: "Rapid Solidification of Metals and Alloys, the Institution of Metallurgists", London, 1982.
3. Ohnaka, I.: *Trans. ISIJ*, **27**, 919 (1987).
4. Yamauchi, T., Nakanori, T., Hasegawa, M., Yabuki, T. and Ohnishi, N.: *Trans. ISIJ*, **28**, 23 (1988).
5. Dancy, T. E.: *I&SM, Dec.*, 25 (1987).
6. Stanek, V. and Szekely, J.: *Metal. Trans.*(B), **14B**, 487 (1983).
7. Miyazawa, K. and Szekely, J.: *Metal. Trans.*(A), **12 A**, 1047 (1981).
8. Kraus, H. G.: *Numerical Heat Transfer*, **10**, 63 (1986).
9. Lee, S. W.: *Korean J. of Chem. Eng.*, **9**, 199 (1992).
10. Lee, S. W.: "Development of Computer Software for Molten Steel and Solidification in Continuous Casting", SHI, Jan., 1993.
11. Crank, J.: "Free and Moving Boundary Problems", Clarendon Press, Oxford, 1984.
12. Voller, V. R., Cross, M. and Markatos, N. C.: *Int. J. Num. Meths. Eng.*, **24**, 271 (1987).
13. Shyy, W., Tong, S. S. and Correa, S. M.: *Numerical Heat Transfer*, **8**, 99 (1985).
14. Braaten, M. and Shyy, W.: *Numerical Heat Transfer*, **9**, 559 (1986).
15. Anderson, D. A., Tannehill, H. A. and Pletcher, R. H.: "Computational Fluid Mechanics and Heat Transfer", Hemisphere Publishing Co., 1985.
16. Patankar, S. V.: "Numerical Heat Transfer and Fluid Flow", McGraw-Hill Co., 1980.
17. Chen, Y. S.: "A Computer Code for Three-Dimensional Incompressible Flows Using Nonorthogonal Body-Fitted Coordinates Systems", NASA CR-17 8818, Mar., 1986.
18. Carnahan, B., Luther, H. A. and Wilkes, J. O.: "Applied Numerical Methods", John Wiley and Sons, New York, 1969.